15th Canadian Masonry Symposium
Ottawa, Canada
June 2-5, 2025

# Influence of the Horizontal-to-Vertical Compressive Strength Ratio of Hollow Clay Bricks on the In-Plane Lateral Loading Behaviour of Unreinforced Masonry Walls

**Inzunza-Araya Ernesto[i], Saloustros Savvas[ii], and Beyer Katrin[iii]**

## ABSTRACT

Masonry walls are critical structural elements in buildings subjected to seismic actions. Their seismic performance is strongly influenced by the mechanical properties of the masonry units, particularly the vertical and horizontal compressive strengths of the bricks. During an earthquake, damage in unreinforced masonry (URM) walls initiates with cracking at the head and bed joints and can propagate through the bricks, affecting the overall drift capacity. Although current design recommendations recognize the possible impact of horizontal compressive strength, its effect on deformation capacity has not been extensively investigated. A previous experimental study explored the seismic response of URM shear walls, primarily analyzing shear strength, ultimate drift, effective stiffness, and failure mechanisms. The work presented here expands on previous research by incorporating additional experimental data and providing a more detailed evaluation of deformation capacity at multiple limit states, from initial cracking to axial load collapse. Six shear-compression tests were conducted on URM walls built with vertically perforated clay bricks and standard cement mortar, using three types of bricks with similar vertical strength but varying compressive strength ratios (0.09, 0.20, and 0.29). The walls (1.5 m long, 2.0 m high, 0.25 m thick) were tested under two levels of compression load with double-bending boundary conditions to promote shear-controlled failure. Beyond the assessment of ultimate drift, this study also examines the maximum crack widths at different limit states and their implications for deformation capacity. The experimental results highlight variations in failure mechanisms and provide new insights into the relationship between the horizontal-to-vertical compressive strength ratio and the seismic performance of masonry walls. These findings contribute to a better understanding of local damage progression and its correlation with global structural behavior, offering valuable data for refining design approaches for modern URM structures.

## KEYWORDS

Unreinforced masonry, drift capacity, hollow clay bricks, experimental testing, seismic performance

---

[i] Doctoral Assistant, EPFL EESD, Lausanne, Switzerland, ernesto.inzunza@epfl.ch
[ii] Scientist, EPFL EESD, Lausanne, Switzerland, savvas.saloustros@epfl.ch
[iii] Associate Professor, Lausanne, Switzerland, katrin.beyer@epfl.ch

## INTRODUCTION

The seismic performance of unreinforced masonry (URM) walls depends on the mechanical properties of the masonry units, which influence their deformation capacity, failure mechanisms, and overall structural behavior. In modern masonry construction, hollow clay bricks are widely used, offering a variety of geometric and mechanical characteristics that can significantly affect their seismic response [1]. Shear walls, as the primary lateral load-resisting elements in masonry buildings, experience both vertical and horizontal forces during an earthquake. Consequently, their damage progression—initially through mortar joints and later through the bricks—can be strongly influenced by the mechanical properties of the units, particularly their vertical and horizontal compressive strengths.

In fact, the in-plane shear capacity models for URM masonry developed by Ganz and Thürlimann [2-3] and continued by Mojsilovic [4-5], consider both the vertical and horizontal compressive strength of masonry. This approach represents the load bearing mechanism of walls by vertical and inclined stress fields, being the inclined also dependent on the horizontal strength of the masonry. Moreover, Eurocode 6 [6] states that the compressive strength of masonry can be computed from the compressive strength of the units in the same loading direction. For this reason, the horizontal strength of the units plays a role in the shear strength of the masonry. When the horizontal-to-vertical strength ratio is small, masonry units may be more vulnerable to crushing in the horizontal direction affecting the robustness of masonry walls.

Although these effects are acknowledged in design guidelines, they are not treated equivalently. The European design code [7] introduces minimum requirements for the horizontal compressive strength of bricks ($f_{bh}$) but leaves it as a Nationally Determined Parameter (NDP) due to limited experimental evidence. In contrast, the Swiss standard [6] does not explicitly consider horizontal brick strength. Previous studies [8] have highlighted the need for further investigation into the role of unit typology, as its influence on deformation capacity remains unclear, particularly for hollow clay bricks with grooves or tongues. A previous experimental campaign [9] investigated the seismic behavior of URM shear walls built with hollow clay bricks, focusing on key parameters such as shear strength, ultimate drift, effective stiffness, and failure mechanisms. That study presented five out of six planned cyclic shear-compression tests, identifying trends in drift capacity but leaving some aspects, such as the role of horizontal brick strength, only partially addressed. The present study completes the test matrix by incorporating the sixth specimen and expands the scope of analysis to provide a more comprehensive evaluation of drift capacity across different limit states—from onset cracking to axial load collapse.

In addition to revisiting key parameters from the previous study, this paper introduces new aspects of the seismic response of URM walls. A detailed assessment of drift capacity at multiple limit states is provided, rather than focusing only on ultimate drift. Furthermore, maximum crack widths at these limit states are reported, along with their impact on deformation capacity. By extending the dataset and refining the evaluation of material properties, this study aims to improve the understanding of how brick compressive strengths influence global structural performance.

## EXPERIMENTAL SETUP

The experimental campaign was conducted at the Structural Engineering Laboratory of EPFL, testing six unreinforced masonry walls (1.54 m long × 2.0 m high × 0.25 m thick) under shear-compression with double-bending boundary conditions (shear span ratio of 0.5). The walls were built using three types of vertically perforated clay bricks (300 mm long × 250 mm wide × 190 mm high) with identical dimensions but different mechanical properties (Figure 1). Standard M15 cement mortar was used with 10 mm thick, fully filled joints.

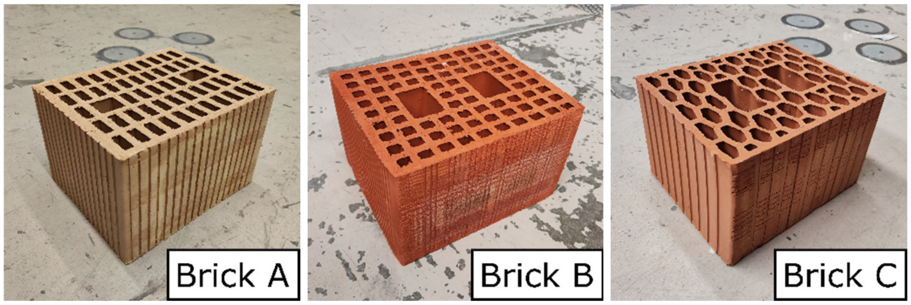


**Figure 1: Bricks used on walls tested (adapted from [9])**

Bricks A and B (45% void ratio) fall under Eurocode 6 [6] category 2, while Brick C (60% void ratio) belongs to category 3. Table 1 presents their material properties, including the normalized vertical ($f_b$) and horizontal ($f_{bh}$) compressive strengths, as well as the horizontal-to-vertical compressive strength ratio ($f_{bh}/f_b$) ratio and the compressive strength of the masonry made with each brick ($f_m$). Brick A have the highest $f_{bh}/f_b$ (0.29), followed by Brick B (0.20) and Brick C (0.09).

**Table 1: Material properties of bricks and masonry (modified from [9])**

| Brick type | $f_b$ [MPa] | $f_{bh}$ [MPa] | $f_{bh}/f_b$ | $f_m$ [MPa] |
|---|---|---|---|---|
| Brick A | 30.40 | 8.70 | 0.29 | 7.04 |
| Brick B | 18.90 | 3.70 | 0.20 | 6.89 |
| Brick C | 22.20 | 2.00 | 0.09 | 5.27 |

Table 2 summarizes the notation used to identify each wall with their respective control variables, covering two levels of compression load expressed in terms of axial load ratio (ALR) and three types of bricks characterized by their $f_{bh}/f_b$. ALR is defined as the ratio between the axial stress applied on the wall ($\sigma$) and the masonry strength ($f_m$). Although the focus is to study the effect of the brick mechanical properties, the variation in level of compression load was included because it has also been identified as an influencing variable on the drift capacity [13]. The combination of these two variables presents an interesting scenario for evaluating different damage mechanisms and their consequences in terms of deformation capacity.

**Table 2: Control variables in wall specimens (adapted from [9])**

| Wall ID | $f_{bh}/f_b$ | ALR ($\sigma/f_m$) |
|---|---|---|
| LfBW0.1 | 0.09 | 0.1 |
| HfBW0.1 | 0.20 | 0.1 |
| MW0.1 | 0.29 | 0.1 |
| LfBW0.2 | 0.09 | 0.2 |
| HfBW0.2 | 0.20 | 0.2 |
| MW0.2 | 0.29 | 0.2 |

Figure 2 contains a global view of the shear-compression test identifying the main elements of the test setup and instrumentation. Each wall was fixed to a reinforced concrete footing and fastened to the strong floor. Loads were applied via a steel beam at the top, with out-of-plane movement restricted by timber guides. A horizontal actuator applied cyclic displacement-controlled loading, while two vertical actuators maintained constant axial force and the double bending boundary conditions. The horizontal displacement followed a predefined drift protocol with two cycles per level, continuing until axial load collapse. The horizontal loading always started in the positive direction, which coincides with the north, and then the negative direction, which coincides with the south. The drift levels implemented in the horizontal loading protocol were: 0.025%, 0.05%, 0.10%, 0.15%, 0.20%, 0.30%, 0.40%, 0.50%, 0.60%, 0.80%, 1.00%.

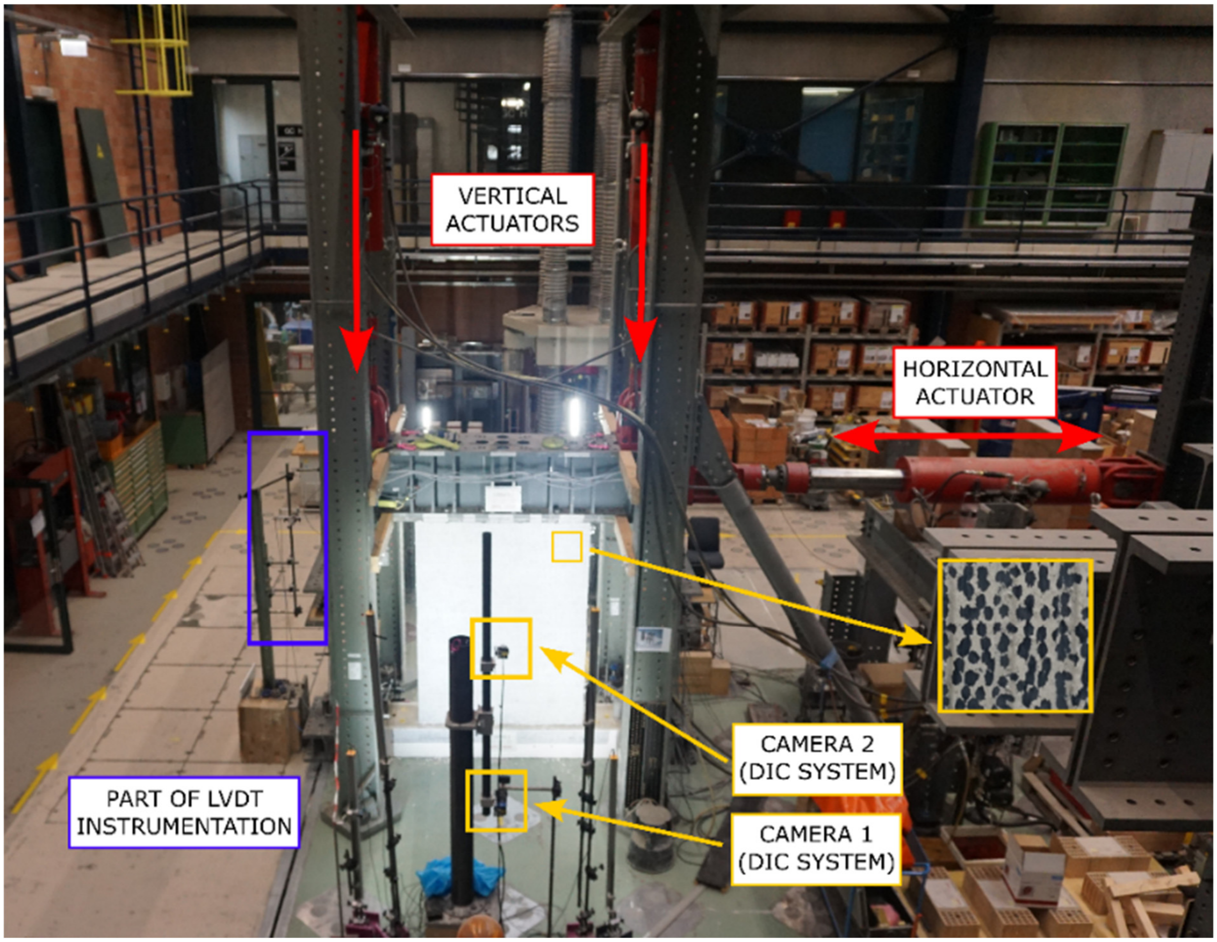


**Figure 2: General setup implemented in each shear-compression test**

Instrumentation included 13 wired sensors: LVDTs to track base sliding, rocking, top displacement, and brick elongation; string pots for beam displacement (axial deformation of the wall); and inclinometers for in-plane and out-of-plane beam rotation. Digital Image Correlation (DIC) was performed on one painted and speckled wall surface using a stereo-camera system of two 28.8 Megapixel digital cameras capturing grayscale images every five seconds.

## Experimental Results and Discussion

Figure 3 illustrates the in-plane hysteretic behavior of six masonry walls, as captured through DIC. The horizontal force is represented as shear stress (in MPa), calculated by dividing the applied force by gross cross-sectional area of the wall. To ensure accuracy, the top horizontal displacement has been corrected to exclude any sliding or rocking effects. The drift (in %) is then obtained by normalizing this displacement by the total wall height. The graphs display the hysteresis envelopes for both loading directions, highlighted in blue. The ultimate drift ($\delta_u$) is marked with red dots on the envelope curves and corresponds to the point where the shear strength of the wall degrades to 80% of its peak shear stress, $\tau_{max}$.

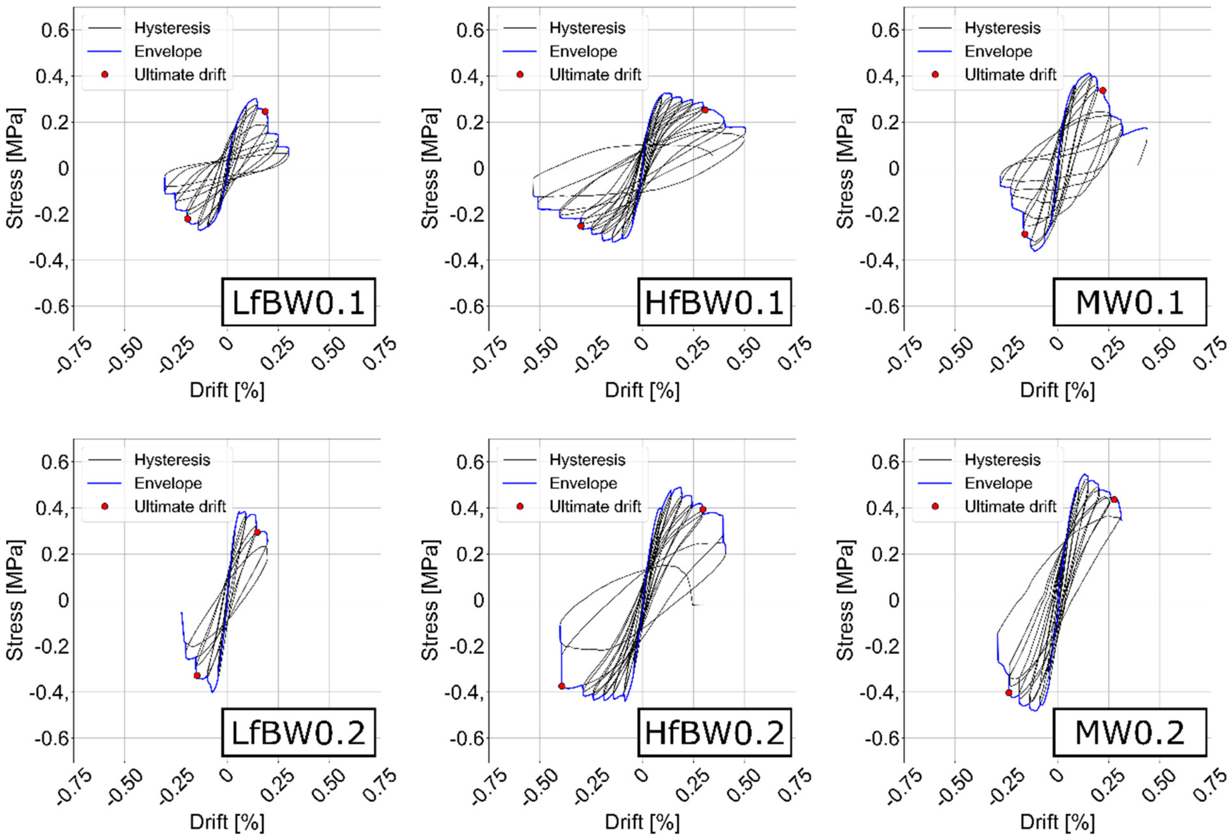


**Figure 3: Hysteresis curve of the six walls tested (adapted from [9])**

Bilinear curves can be determined from hysteresis envelopes, and they are characterized by means of three parameters: the effective stiffness ($k_{eff}$), the equivalent bilinear strength ($\tau_{bil}$) and the ultimate drift ($\delta_u$, defined in the previous paragraph). The effective stiffness is calculated as the secant stiffness intersecting the envelope curve at 70% of the peak shear stress ($\tau_{max}$) within the pre-peak range. The equivalent bilinear strength is taken as the magnitude of the shear stress for which the area under the envelope curve is equal to the area under the bilinear curve within the drift range [0, $\delta_u$].

**Table 3: Bilinear parameters of tested walls (modified from [9])**

| Wall ID | $k_{eff}^{AVG}$ [MPa/%] | $\tau_{bil}^{AVG}$ [MPa] | $\delta_u$ [%] |
|---|---|---|---|
| LfBW0.1 | 4.19 | 0.26 | 0.19 |
| HfBW0.1 | 5.04 | 0.30 | 0.31 |
| MW0.1 | 6.00 | 0.35 | 0.22 |
| LfBW0.2 | 8.01 | 0.36 | 0.15 |
| HfBW0.2 | 5.80 | 0.43 | 0.39 |
| MW0.2 | 6.11 | 0.48 | 0.28 |

Table 3 contains the average effective stiffness ($k_{eff}^{AVG}$), determined as the average of the $k_{eff}$ in both loading directions; the average equivalent bilinear strength ($\tau_{bil}^{AVG}$), result of averaging the $\tau_{bil}$ in both loading directions; and the $\delta_u$ (or drift capacity) considered as the maximum ultimate drift between the positive and negative directions, following the same approach proposed by Beyer et al. [10].

### Effect on Effective Stiffness

When different brick types are observed, the effective stiffness decreases when decreasing $f_{bh}/f_b$ for ALR = 0.1, but not a clear correlation is identified for ALR = 0.2. For all brick types, the effective stiffness increased with increasing ALR. Brick A increases 1.8% its average effective stiffness, Brick B increases 15.1%, and Brick C increases 91.2% with increasing ALR.

### Effect on Shear Strength

A decrease in the $f_{bh}/f_b$ results in a decrease of the shear strength. In particular, the reduction of the $f_{bh}/f_b$ from 0.29 to 0.20 results in a drop of the shear strength of 14.3% for ALR = 0.1, and 10.4% for ALR = 0.2. Similarly, when reducing the $f_{bh}/f_b$ from 0.20 to 0.09 the shear strength decreases 13.3% for ALR = 0.1, and 16.3% for ALR = 0.2. The increase in the ALR resulted in an increase of the shear strength independently of the $f_{bh}/f_b$: 37.1%, 43.3% and 38.5% for Brick A, Brick B and Brick C, respectively.

### Effect on Ultimate Drift

The $f_{bh}/f_b$ does not show a consistent correlation with the ultimate drift for both ALR. A decrease in the $f_{bh}/f_b$ from 0.29 to 0.20 resulted in an increase of $\delta_u$ in 40.9% for ALR = 0.1 and 39.3% for ALR = 0.2. Conversely, a decrease in the $f_{bh}/f_b$ from 0.20 to 0.09 caused a decrease of the $\delta_u$ by 38.7% for ALR = 0.1 and by 61.5% for ALR = 0.2. The effect of the ALR on the drift capacity is not the same for all the brick types. Brick A experienced an increment of $\delta_u$ of 27.3%, Brick B an increment of 25.8%, but Brick C a reduction of 21.1%.

### Effect on Failure Mode

Figure 4 displays the condition of the walls at the last target drift level in accordance with the test protocol before the axial load collapse. All the walls are aligned in a north-south orientation, corresponding to left and right. In five out of six walls the failure mechanism is diagonal shear cracking, which is typical in shear-controlled walls.

Crack patterns varied among walls tested under ALR = 0.1. While all specimens exhibited primary diagonal cracks in both loading directions, only HfBW0.1 showed a fully corner-to-corner trajectory. In contrast, MW0.1 and LfBW0.1 had asymmetrical crack intersections shifted toward the top left. MW0.1 developed a crack from the second row above the base that changed direction after intersecting another diagonal crack, forming a horizontal pattern near the top right. LfBW0.1, on the other hand, exhibited a more vertical crack path extending toward the top center, with significant crushing and damage in the uppermost brick row. At this drift level, cracks transitioned from a stepped pattern along mortar joints to diagonal fractures passing through the brick units. Additionally, brick shell detachment was observed, exposing internal webs and indicating lateral brick deformation, particularly concentrated at the top row in LfBW0.1.

For walls tested under ALR = 0.2, diagonal cracking was evident in both orientations, but with distinct progression sequences. In MW0.2, fine diagonal cracks initially formed an "X" shape, later transitioning into wider vertical cracks, resulting in a mixed "X-H" failure pattern. Conversely, HfBW0.2 first developed vertical cracks along head and bed joints before diagonal cracks became dominant, gradually evolving into a corner-to-corner trajectory.

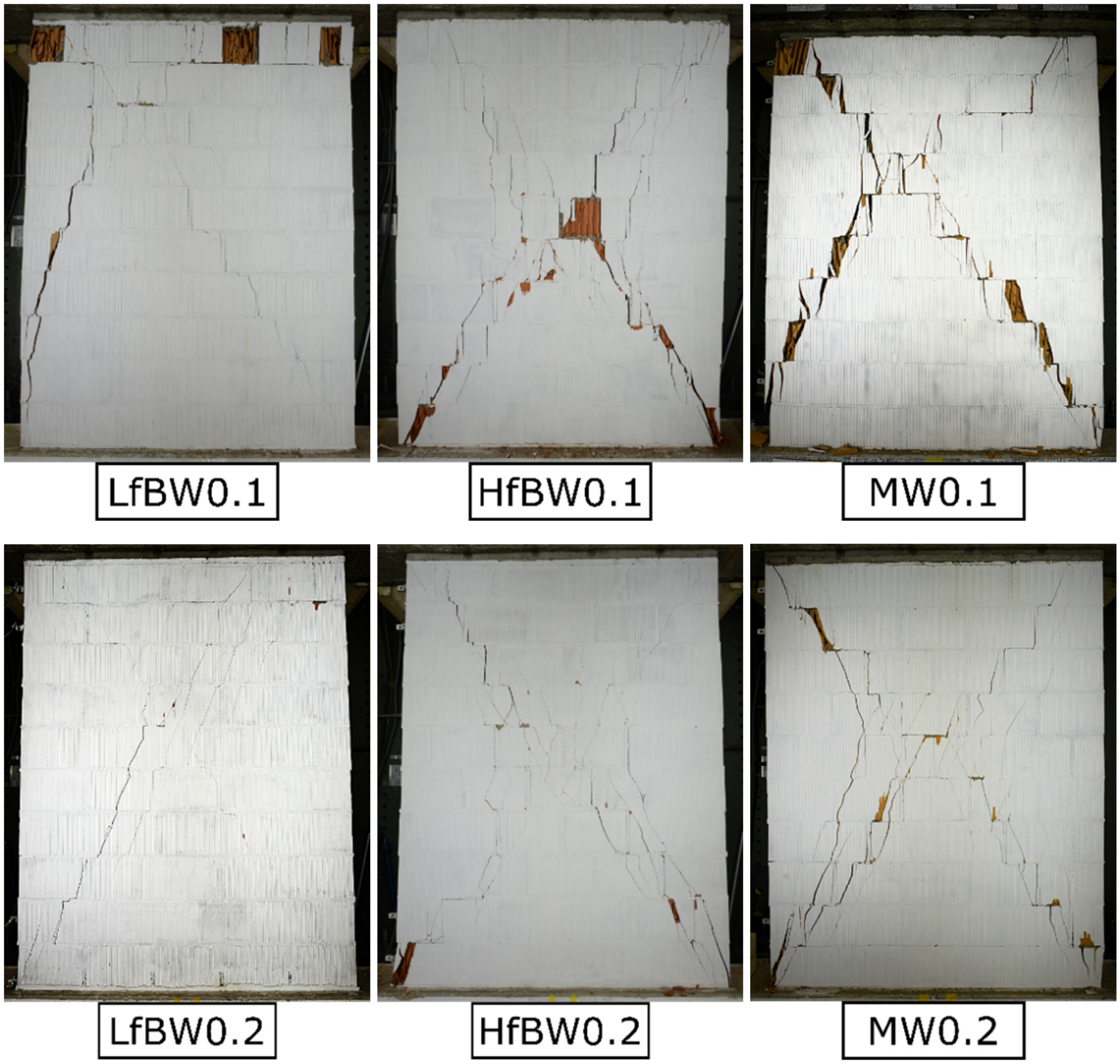


**Figure 4: Condition before axial load collapse of the six walls tested (adapted from [9])**

This behavior under higher ALR suggests two key influences: increased compression stresses altering the failure mechanism, leading to vertical cracking typical of compression failures, and the lower $f_{bh}/f_b$ making bricks more susceptible to cracking, thereby affecting damage progression at earlier stages. A similar influence of $f_{bh}/f_b$ was observed in LfBW0.1, where damage concentrated on brick units, modifying the failure mode.

### Effect on Damage Progression

With the aim of facilitating the analysis for the drift capacity and damage propagation, seven limit states (LS) have been defined. The limit states cover the whole evolution of damage from the onset cracking to the condition just before axial load collapse.

- LS-0 (onset cracking): first crack observed according to visual inspection.
- LS-1 (shear strength): maximum shear force reached during the test.
- LS-2 (ultimate drift): post-peak regime. Drop in 20% of the maximum shear force.
- LS-3 (drop 30% force): post-peak regime. Drop in 30% of the maximum shear force.

- LS-4 (drop 40% force): post-peak regime. Drop in 40% of the maximum shear force.
- LS-5 (drop 50% force): post-peak regime. Drop in 50% of the maximum shear force.
- LS-6 (maximum drift): post-peak regime. Maximum drift recorded before axial load collapse.

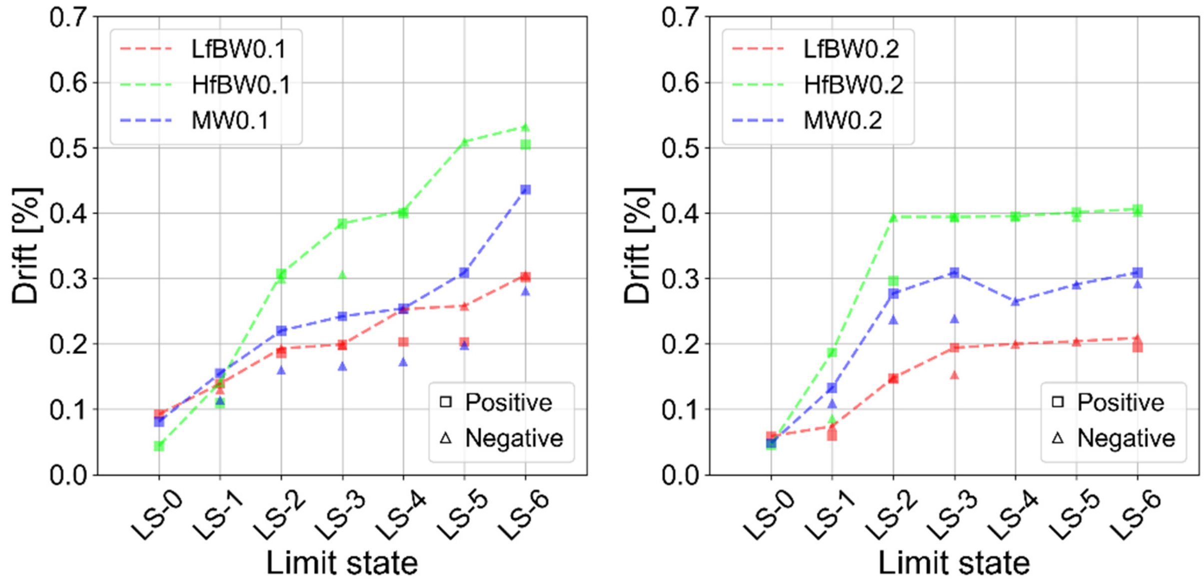


**Figure 5: Deformation capacity at different limit states**

Figure 5 shows the drift attained at all seven limit states for each wall. The red dashed line denotes walls with the lowest $f_{bh}/f_b$ (0.09), the green line indicates an intermediate $f_{bh}/f_b$ (0.20), and the blue line represents the highest $f_{bh}/f_b$ (0.29). The graph on the left includes the walls subjected to ALR = 0.1, while the graph on the right contains the walls subjected to ALR = 0.2. For both levels of compression load it is observed that the wall with intermediate $f_{bh}/f_b$ develops the highest deformation capacity throughout the post-peak range (from LS-1 onwards). On the other hand, the wall with the smallest $f_{bh}/f_b$ develops the lowest deformation capacity along the same range.

The progression of the deformation capacity depending on the level of compression load is also different. When the ALR is lower, the deformation capacity tends to increase gradually from LS-0 to LS-6. In contrast, when the ALR increases, the deformation capacity increases until it reaches the ultimate drift (LS-2), at which point it experiences a sudden failure, causing the ultimate drift to coincide with the maximum drift. In the graph on the right, this last feature is reflected in the curves that maintain a steady drift after LS-2.

### Effect on Crack Width

To supplement the qualitative description of the cracking pattern and failure mechanism, a crack analysis was performed on the walls, which allowed for the identification and quantification of cracks on the wall's surface. The crack opening was determined by the open-source software ACDM (automated crack detection and measurement) [11-12]. The computations were executed using as input the measurements obtained from DIC performed by the software VIC-3D. By using the principal strain fields and calibrating thresholds for the principal strains corresponding to the onset of cracking for each wall, the crack openings in the normal (crack width) and tangential (crack slip) directions were extracted. The threshold limits have been selected according to the first crack observed during the shear-compression tests. With this methodology, the crack pattern with respective crack opening can be determined at any moment of the test.

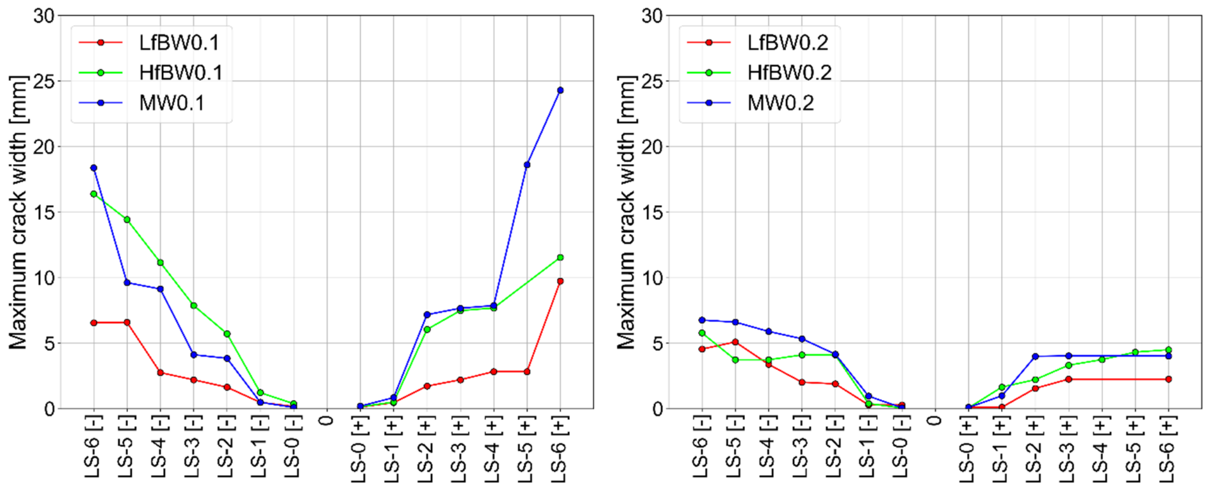


**Figure 6: Maximum crack width evolution**

Figure 6 displays the maximum crack width extracted at each limit state for the six walls tested. On the left it has been grouped the walls subjected to lower ALR, and on the right the walls subjected to higher ALR. The color notation is the same as the one described in Figure 5 (red, green and blue for $f_{bh}/f_b$ = 0.09, 0.20 and 0.29 respectively). It is observed that for both levels of compression load the walls built with bricks with the lowest $f_{bh}/f_b$ develop thinner cracks. However, there is not a clear trend for walls developing the largest crack widths. This phenomenon is more clearly noted for walls subjected to ALR = 0.1, where green and blue curves describe higher or lower maximum crack widths depending on the loading direction and the LS.

When comparing the magnitude of the maximum crack width for different level of compression load, the graphs indicate that walls under lower ALR develop higher crack widths. Furthermore, the relationship between LS and maximum crack width is comparable to that between LS and deformation capacity. As shown in Figure 5, for lower ALR, the maximum crack width tends to increase progressively, but for larger ALR, the maximum crack width seems to remain constant after LS-2. This behaviour allows us to correlate the deformation capacity with the ability of developing wider cracks.

## CONCLUSIONS

This experimental study investigated the in-plane response of six masonry walls, analyzing the effects of ALR and the $f_{bh}/f_b$ ratio on stiffness, shear strength, deformation capacity, failure mechanisms, and crack evolution.

### Effective Stiffness

Results show that the effective stiffness decreased when reducing $f_{bh}/f_b$ for ALR = 0.1, but no clear correlation was observed for ALR = 0.2. Regardless of $f_{bh}/f_b$, increasing ALR resulted in higher stiffness. Specifically, Brick A increased by 1.8%, Brick B by 15.1%, and Brick C by 91.2%.

### Shear Strength

The shear strength consistently decreased as $f_{bh}/f_b$ was reduced. When $f_{bh}/f_b$ decreased from 0.29 to 0.20, shear strength dropped by 14.3% for ALR = 0.1 and 10.4% for ALR = 0.2. A further reduction from 0.20 to 0.09 led to a 13.3% drop for ALR = 0.1 and 16.3% for ALR = 0.2. Conversely, an increase in ALR resulted in higher shear strength regardless of $f_{bh}/f_b$, with increases between 37-44%

### Ultimate Drift

No consistent correlation was found between $f_{bh}/f_b$ and $\delta_u$ across both ALR levels. A reduction in $f_{bh}/f_b$ from 0.29 to 0.20 increased $\delta_u$ by 40.9% for ALR = 0.1 and 39.3% for ALR = 0.2. However, a further decrease in $f_{bh}/f_b$ from 0.20 to 0.09 led to a significant drop in $\delta_u$ by 38.7% for ALR = 0.1 and 61.5% for ALR = 0.2. The effect of ALR on drift capacity varied among brick types: Brick A and Brick B showed increases of 27.3% and 25.8%, respectively, while Brick C exhibited a reduction of 21.1%.

### Failure mechanism

Diagonal shear cracking was the dominant failure mode in five out of the six walls, a characteristic of shear-controlled failure. Under ALR = 0.1, crack patterns varied, with some walls exhibiting asymmetric diagonal cracking and localized crushing in the top brick row (this last phenomenon for the wall with the lowest $f_{bh}/f_b$). For ALR = 0.2, crack progression followed different sequences, with some walls initially developing vertical cracks before transitioning to diagonal failure. Increased compressive stresses under higher ALR altered the failure mechanism, leading to earlier vertical cracking and modifying the overall damage progression.

### Deformation Capacity

Seven limit states were defined to assess the evolution of deformation and damage, from onset cracking (LS-0) to maximum drift before axial collapse (LS-6). The wall with the intermediate $f_{bh}/f_b$ consistently demonstrated the highest deformation capacity in the post-peak range (LS-1 onwards), whereas the lowest $f_{bh}/f_b$ led to the lowest deformation capacity. Under lower ALR, deformation increased progressively across all LS, while for higher ALR, failure occurred suddenly at LS-2, with ultimate drift coinciding with maximum drift.

### Crack Width Evolution

Crack width measurements were obtained using automated detection software (ACDM) based on DIC strain fields. Walls with the lowest $f_{bh}/f_b$ developed thinner cracks, though not a clear trend was observed between the two higher $f_{bh}/f_b$ ratios, especially for ALR = 0.1. Walls under lower ALR exhibited wider cracks, and the evolution of crack width followed a similar trend to deformation capacity. For lower ALR, crack widths increased progressively, whereas for higher ALR, crack widths remained nearly constant after LS-2, correlating with the observed deformation trends.

### Final Remarks

The study highlights the significant influence of $f_{bh}/f_b$ and ALR on the seismic response of masonry walls, affecting bilinear parameters, as well as the evolution of the damage reflected on the deformation capacity and the crack width. This work provides a valuable example of how a crack analysis can contribute to characterize the mechanics behind the seismic behaviour. Firstly, the obtention and representation of cracking pattern can be effectively used to calibrate numerical models. Additionally, the connection between crack magnitudes and damage condition could have an important application on the safety assessment.

## ACKNOWLEDGEMENTS

The work presented has been financed through the research grant BAFU-D-828B3401/337 and titled "Continuing the development of drift capacity models and force reduction factors for modern masonry buildings in Switzerland" by the Swiss Federal Office for the Environment (OFEV). The authors would like to thank the team of the Structural Engineering Laboratory at EPFL for their unvaluable technical support.

## REFERENCES


[1] Tomaževič, M., Lutman, M., Bosiljkov, V. (2006). "Robustness of hollow clay masonry units and seismic behaviour of masonry walls". *Construction and Building Materials*, 20, 1028–1039.

[2] Ganz, H.R. (1985). "Masonry walls subjected to normal and shear forces (in German)". Ph.D. Thesis. Institute of Structural Engineering, ETH Zurich, Zurich, Switzerland.

[3] Ganz, H.R., Thürlimann, B. (1988). "Design of masonry walls under normal force and shear". In: *Proceedings of the 8th International Brick/Block Masonry Conference*, Dublin, Ireland, pp. 1447–1457.

[4] Mojsilović, N. (2011). "Strength of masonry subjected to in-plane loading: A contribution," Int. J. Solids Struct., vol. 48, no. 6, pp. 865–873, Mar. 2011.

[5] Mojsilović, N. (1995). "Response of masonry subjected to combined actions (in German)". *Tech. Rep.*, ETH Zürich, Zurich, Switzerland.

[6] SIA. (2015). "SIA 266: Masonry". Zürich, Switzerland: Swiss Society of Engineers and Architects.

[7] CEN (2005). "Eurocode 6- Design of masonry structures - Part 1-1: General rules for reinforced and unreinforced masonry structures". Brussels, Belgium.

[8] Beyer, K., Wilding, B. V., Rezaie, A. (2022). "Proposed changes to the masonry chapter in EC8 Part 1 – Background document for the masonry chapter in EC8 Part 1". *Tech. Rep. (version number: V1.2b)*.

[9] Inzunza Araya, E., Saloustros, S., Beyer, K. (2025). "Influence of the horizontal-to-vertical compressive strength of hollow clay bricks on the in-plane drift capacity of unreinforced masonry walls". *18th International Brick and Block Masonry Conference (IB2MaC 2024)*, Birmingham, UK.

[10] Beyer, K., Araya, E.A.I., Saloustros, S. (2022a). "Drift Capacity Models for the New Masonry Chapter of Eurocode 8 Part 1-2". *Proc., Earth and Environmental Sciences*, Bucharest, Romania.

[11] Gehri, N., Mata-Falcón, J., Kaufmann, W. (2020). "Automated crack detection and measurement based on digital image correlation". *Construction and Building Materials*, 256, 119383.

[12] Gehri, N., Mata-Falcón, J., Kaufmann, W. (2022). "Refined extraction of crack characteristics in largescale concrete experiments based on digital image correlation". *Engineering Structures*, 251, 113486.

[13] Wilding, B. V., Beyer, K. (2018). "Analytical and empirical models for predicting the drift capacity of modern unreinforced masonry walls". *Earthquake Engineering & Structural Dynamics*, 47 (10), 2012–2031.